High-power isolator for the 10-μm region employing interband Faraday rotation in germanium*

C. R. Phipps, Jr.† and S. J. Thomas†

Los Alamos Scientific Laboratory, University of California, Los Alamos, New Mexico 87544
(Received 7 April 1975)

Interband Faraday rotation in intrinsic germanium has been employed to construct a room-temperature optical isolator for use in the intermediate infrared region. The device was tested at 9.55- and 10.59-μm wavelengths, and exhibited an isolation level of 41 dB at 10^6 W cm^{-2}. The rotation is shown to be relatively insensitive to temperature at the two wavelengths and linear in magnetic field intensity up to 83 kG. The isolator figure of merit is about 60 deg per dB attenuation.

PACS numbers: 42.60.L, 78.20.L

I. INTRODUCTION

High-power laser oscillator-amplifier systems are now being developed at several laboratories with the intent of initiating deuterium-tritium thermonuclear reactions in small fuel pellets by means of a laser-driven implosion.[1] A crucial element in the design of such systems is the provision of adequate interstage isolation. Devices built for this purpose satisfy two important requirements in a laser system design.

(i) *Prevention of spontaneous lasing*: Unwanted oscillation in the amplifier chain must be suppressed. Net gain must be reduced below threshold except during a limited time interval in which the desired signal is to be amplified.

(ii) *Suppression of retrodirected signals*: After the amplification interval, system gain must be further depressed to adequately limit strong retrodirected signals. These may arise as output reflections from windows or targets, or inadvertently as the full output of other laser systems in multiple-beam irradiation experiments. Suppression of such signals is necessary to prevent optical damage to oscillator components and desirable to prevent multiple illumination pulse echoes at the target.

For early laser fusion experiments, the greatest effort is being directed to laser development at the 1.06- and 10.6-μm wavelengths. While isolation techniques are generally well understood at the shorter wavelength,[2,3] only nonlinear absorbers have been made to work effectively in attempts to isolate large CO_2 laser systems.[4] The Stark, Pockels, and Faraday effects have also been employed or studied for this application.[5–7] These approaches are compared in Table I.

Presently, the two most promising candidates for optical isolators in the 10-μm region would appear to be devices based on the Faraday or Pockels effects. The available electro-optic materials limit the latter to 1- or 2-cm apertures, and cost will remain an important consideration when larger crystals become available.

Faraday effect devices satisfy the two main requirements for CO_2 laser system isolation, but have not been fully developed for this application. In this paper, we report the design and testing of a room-temperature high-power Faraday rotation isolator for the 10-μm region. This isolator exhibited a broad-band isolation capability, in excess of 40 dB for high intensities at a specific wavelength. The device can be scaled to apertures as large as 30 cm. Unlike other devices reported for this application,[7–9] it is based on bound-carrier (interband) Faraday rotation in intrinsic germanium.

In what follows, Sec. II provides a theoretical basis for subsequent discussions, while Sec. III summarizes our reasons for using interband rather than free-carrier rotation in addressing the 10-μm isolation problem. In Sec. IV, we explain why germanium was selected for the rotation medium, describe the isolator design, and present experimental results. In Secs. V and VI, respectively, we discuss these results and suggest directions for further work.

II. THEORY OF FARADAY ROTATION

The plane of polarization of an electromagnetic wave

TABLE I. Evaluation of isolation techniques for CO_2 laser systems.

Isolation technique \ Criterion	Relative cost	Aperture	Bandwidth	Figure of merit[a]	Required field uniformity
Nonlinear absorption	Low	Large	Generally restricted	Poor	*N/A*
Pockels devices	High	Small	Broad	Excellent	Moderate
Stark devices	Moderate	Moderate	Restricted	Poor	Stringent
Faraday devices	Moderate	Large	Broad	Execellent	Moderate

[a]The figure of merit is a suitably defined ratio of isolation level to insertion loss.

is rotated about the propagation axis in a medium which exhibits different phase velocities c/n_+ (c/n_-) for right (left) circularly polarized waves [rcp (lcp)]. If positive rotation is defined as right-handed looking along the propagation vector, the specific rotation is given by

$$\theta = \tfrac{1}{2}k_0(n_- - n_+) \text{ rad cm}^{-1}. \tag{1}$$

Here, n is the real part of the complex refractive index $\eta = n - i\kappa$ and $\mathbf{k}_0$ is the vacuum propagation vector. Faraday rotation describes the case where this rotatory dispersion is magnetically induced. The oscillations of both free and bound charges in the magnetized medium contribute to the dispersion, and give the rotation a definite absolute "sense", independent of the direction $\mathbf{k}$ of propagation. In the propagation vector frame, however, the rotation appears to reverse when $\mathbf{k}$ reverses. The specific rotation is linear in the component $\mathbf{B}\cdot\hat{\mathbf{k}} = B_z$ of the magnetic field for sufficiently small fields; the constant of proportionality is the Verdet coefficient,

$$V = \theta/B_z \text{ rad cm}^{-1}\text{G}^{-1}. \tag{2}$$

The equation of motion for a classical oscillator of charge q_j, mass m_j, and resonant frequency ω_j, driven by a radiation field $\mathbf{E}(\omega)$ in a static magnetic field is[10]

$$\ddot{\mathbf{r}}_j + (\dot{\mathbf{r}}_j \times \omega_{cj}) + \nu_j \dot{\mathbf{r}}_j + \omega_j^2 \mathbf{r}_j = (q_j \mathbf{E}/m_j)\exp(i\omega t). \tag{3}$$

Here,

$$\omega_{cj} = -\, q_j \mathbf{B}/m_j c \tag{4}$$

is the vector cyclotron frequency. In Eq. (3), ν_j is a phenomenological collision frequency representing damping.

The solution of Eq. (3) yields a complex refractive index given by

$$\left(\frac{\eta_\pm}{n_0}\right)^2 = \left(1 + \frac{4\pi\sigma_\pm}{i\omega n_0^2}\right) = 1 + \sum_j \left(\frac{\omega_{pj}^2/n_0^2}{\omega_j^2 - \omega(\omega \mp \omega_{cj} - i\nu_j)}\right), \tag{5}$$

where $\omega_{pj}^2 = 4\pi N_j e^2/m_j$ is the plasma frequency, n_0 is $\text{Re}(\eta)$ for $B = 0$, and $\sigma_\pm$ is the complex conductivity of the medium, for rcp and lcp wave components. In the limit of few collisions ($\nu/\omega \ll 1$) and small fields ($\omega_c/\omega \ll 1$), the Faraday rotation due to an assembly of oscillators can be written[11]

$$\theta(\omega) \approx \frac{1}{2n_0 c} \sum_j \left(\frac{\omega_{pj}^2 \omega_{cj} \omega^2}{(\omega_j^2 - \omega^2)^2}\right), \tag{6}$$

where $|\eta_- - \eta_+|/n_0 = O(\theta/k_0) \ll 1$ and $\kappa/n = O(\alpha/k_0) \ll 1$, and $\alpha = 2k_0\kappa$ is the intensity absorption coefficient.

Differentiation of Eq. (5) under the preceding assumptions yields the Becquerel formula,[12]

$$\theta(\omega) \approx -\frac{\omega\omega_c}{2c}\frac{d\eta}{d\omega}, \tag{7}$$

which emphasizes the roles played by natural dispersion and by the magnetic field in Faraday rotation.

Two distinct behaviors for each oscillator species can be seen in Eq. (6). For $\omega \ll \omega_j$ (the low-frequency limit of interband rotation), $\theta \sim \omega^2$, while for $\omega \gg \omega_j$ (the free-carrier limit), $\theta \sim \omega^{-2}$. For free carriers, the collision frequency is given by

$$\nu_F = ge/\mu m_F, \tag{8}$$

where m_F is the free-carrier effective mass.

Similarly, for few collisions and small fields, the absorption coefficient which results from Eq. (5) is given by

$$\alpha(\omega) \approx \frac{1}{n_0 c} \sum_j \left(\frac{\omega_{pj}^2 \nu_j \omega^2}{(\omega_j^2 - \omega^2)^2}\right). \tag{9}$$

A figure of merit for rotator materials is the rotation per unit loss. Equations (6) and (9) give, for one species,

$$Q = |\theta/\alpha| = \tfrac{1}{2}|\omega_c/\nu|. \tag{10}$$

In particular, for free carriers, making use of Eq. (8),[13]

$$Q_F = \mu B/2gc. \tag{11}$$

The best free-carrier rotator can therefore be selected from a table of mobilities.

For the interband case, the summation $\sum_j$ is performed over pairs of initial and final Landau states k and k' produced by magnetic field quantization. The density $N_{kk'}$ used in computing $\omega_{pkk'}^2$ is the oscillator strength for the transition kk', related to the momentum matrix element $P_{kk'}$ and transition frequency $\omega_{kk'}$, by[10]

$$N_{kk'} = \frac{|P_{kk'}|^2}{m\hbar\omega_{kk'}}. \tag{12}$$

The collision frequency $\nu_{kk'}$ is the reciprocal lifetime of a given transition. Spin-orbit coupling necessitates multiplication of Eqs. (6), (7), (9), and (10) by a factor $\frac{1}{2}(g_c + g_v)$, where g_c and g_v are the effective gyromagnetic ratios for the conduction and valence bands. This factor determines the sign of interband rotation.

Detailed calculations of interband Faraday rotation have been done for several classes of nonmagnetic semiconducting materials with cubic crystal lattices, including the group-IV, III-V, and II-VI compounds.[14-18] The works of Roth,[14] Boswarva and Lidiard,[15] and Halpern, Lax, and Nishina[16] established the theoretical basis for these calculations.

For our purposes, only the region $\omega < \frac{1}{2}\omega_g$ is interesting, since high-power isolators must be designed to avoid two-photon absorption. Further, we will only be interested in the asymptotic behavior of rotation due to the direct allowed transitions. The effect of excitons and of the indirect (phonon-assisted) transitions can be ignored well below the gap[10,14,15,19] while intraband transitions are avoided by eliminating the free carriers.[10,20,21]

The low-frequency limit for interband rotation due to direct transitions in a cubic crystal is given by[14,22]

$$V_I(\omega \ll \omega_g) = \left(\frac{5\sqrt{2}}{64}\,\frac{m_r^{3/2} e^3 (g_v + g_c)}{n_0 m^3 c^2 \hbar^{5/2}}\right) \times |P|^2 \frac{\omega^2}{\omega_g^{7/2}} \text{ rad cm}^{-1}\text{G}^{-1}, \tag{13}$$

where m_r is the reduced effective mass of the two bands involved and P is the momentum matrix element for the transition. Since cubic crystals are optically isotropic in the absence of an applied magnetic field, it might be

expected that the low-frequency limit of the Faraday effect is also isotropic in these crystals, permitting the use of polycrystalline rotator materials. However, since anisotropy was ignored in the calculations which led to Eq. (13), quantitative assessment of its magnitude must await experimental data.

From Eq. (6), free-carrier rotation is given by

$$V_F(\omega_g \to 0) = \frac{2\pi e^3 \omega^{-2}}{n_0 c^2}\left(\frac{N_e}{m_{Fe}^2} - \frac{N_p}{m_{Fp}^2}\right) \quad \text{rad cm}^{-1}\,\text{G}^{-1} \qquad (13')$$

$$= 1.51\times10^{-20}\,\frac{m^2\lambda_\mu^2}{n_0}\left(\frac{N_e}{m_{Fe}^2} - \frac{N_p}{m_{Fp}^2}\right) \text{deg cm}^{-1}\,\text{kG}^{-1},$$

where λ_μ is the wavelength in μm, and N_e and N_p are the electron and hole densities in cm^{-3}. The contributions of electrons and holes to the total rotation are oppositely directed, although the contrary is often stated in the literature.

III. APPLICATION TO ISOLATOR DESIGN FOR 10.6 μm

We are now in a position to compare the mechanisms of interband rotation and free-carrier rotation in a semiconductor for the purpose of constructing an isolator in the intermediate infrared. It has been shown that InSb is the material of choice for the free-carrier application because of its unusually high electron mobility.[8]

A. Isolation figure of merit

If the refractive indices and absorption coefficients for right and left circularly polarized waves are known functions of frequency, the Kramers-Kronig relations give the Faraday rotation as[23]

$$\theta(\omega) = -\frac{\omega^2}{2\pi n_0}\int_0^\infty \frac{d\omega'}{\omega'}\left(\frac{n_+\alpha_- - n_-\alpha_+}{\omega'^2 - \omega^2}\right). \qquad (14)$$

It is clear that a strong absorption edge, removed from the operating frequency ω, can be equally effective in producing significant rotation at ω as a coincident weak absorption.

Interband rotation well below the energy gap permits this decoupling of rotation and absorption mechanisms, whereas free-carrier rotation does not. In CdTe, for example, at 10.6 μm, absorptions as small as 3×10^{-4} cm^{-1} have been measured,[24] corresponding to a figure of merit of 2000 deg/dB at 84 kG.[25] In contrast, n-type InSb has achieved a figure of merit of 98 deg/dB.[7]

B. Achievable isolation level

An isolator which is ideal except for an average small radial variation $\xi = d\theta/\theta$ in the specific rotation will show a limiting reverse attenuation

$$A = 2.10 + 20\log_{10}(\xi^{-1}). \qquad (15)$$

For example, a 10% variation in doping density in an InSb isolator wafer will limit the achievable isolation level to 22 dB.[9] Suppliers of InSb we contacted would not quote doping uniformities better than 50%. Nonuniform heating will cause an additional inhomogeneity of thermally produced free carriers.

On the other hand, since the density N appropriate to interband rotation is fixed by that of the crystal structure, interband device isolation levels in a uniform magnetic field will be limited by (a) ellipticity due to the slight difference in α_+ and α_-, (b) the Voigt phase shift, and (c) local energy gap variations caused by nonuniform heating. In Appendix A, these effects are discussed in more detail.

C. Multiple-photon absorption

The energy gap in intrinsic InSb varies from 0.18 eV at room temperature to 0.225 eV at 77 °K.[26,27] Impurity concentrations up to 2×10^{17} cm^{-3} cause the gap to increase by $\leq 5\%$.[11] Two 10.59-μm photons have an energy of 0.234 eV, which is nearly coincident with the InSb gap energy at 77 °K, and slightly in excess of the gap energy for higher temperatures. None of the customary CO_2 laser transitions will escape two-photon absorption at sufficient intensities in InSb. The coefficient for this absorption at 10.59-μm wavelength in room-temperature 10^{17}-cm^{-3} n-type InSb is[28]

$$K_2(10.6\ \mu\text{m}) = 16 \pm 5\ \text{cm}^{-1}(\text{MW cm}^{-2})^{-1}. \qquad (16)$$

The threshold for this process is about 10^5 W cm^{-2}.[28] For this reason, InSb is an unsuitable Faraday rotation medium for fusion-oriented CO_2 laser systems, which operate at intensities up to 10^9 W cm^{-2}.[28]

Two-photon absorption in the 9—10-μm region is energetically forbidden in Ge, with an energy gap of 0.65 eV.[11]

D. Thermal effects

The local temperature rise of a rotator medium subsequent to a laser pulse of energy density J_0 joule cm^{-2} is given by

$$\Delta T(x) = 0.24(\alpha J_0/\rho c_p)\exp(-\alpha x)\ ^\circ\text{K}. \qquad (17)$$

Here α is the absorption coefficient, ρ is the density, and c_p the specific heat of the material. The fraction of the pulse energy absorbed by the medium is

$$\Delta W/W_0 \approx \pi/4Q, \qquad (18)$$

for $W/W_0 \ll 1$ and $\pi/4$ total rotation. However, from Eq. (10), $\alpha = \theta Q$. Therefore, modest specific rotation and large figure of merit are desirable to reduce both temperature rise and absorbed energy fraction. For example, if $J_0 = 2$ J cm^{-2}, a single shot will cause a 13 °K temperature rise in InSb (assuming $\alpha = 7.9$ cm^{-1}), but only 0.015 °K in Ge, taking $\alpha = \alpha_p$.

While $dV/V\,dT$ can be made nearly zero for proper doping concentrations in InSb,[8] such large temperature excursions raise questions of heat dissipation and thermal fracture, for InSb or materials of similar absorptivity.[29]

E. Practical constraints

Three additional criteria of a practical nature are of importance in isolator design for large CO_2 laser systems.

(a) *Purity*: In an interband rotator, it is essential to eliminate free-carrier effects in order to achieve minimum absorption and to avoid degradation of rotation uniformity. Resonable limits are that the free-carrier

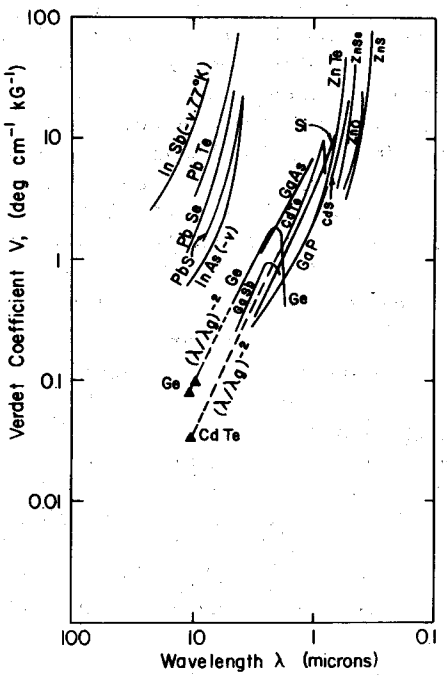

FIG. 1. Room-temperature Verdet coefficients vs wavelength. Sources: CdS: Ref. 30; CdTe: Refs. 25 and 31; GaAs: Ref. 32; GaP: Ref. 33; GaSb: Ref. 34; Ge: Refs. 25 and 35; InAs: Ref. 36; InSb: Ref. 26; PbS, PbSe, and PbTe: Ref. 37; Si: Ref. 38; ZnO, ZnS, ZnTe, and ZnSe: Ref. 30.

rotation be less than 1% of the interband rotation. The consequent purity and temperature limits for a germanium interband rotator are (see Appendix B)

$$N_i \leq 4\times10^{13}\ \text{cm}^{-3} \quad \text{and} \quad T \leq 310\,^{\circ}\text{K}$$

(b) *Aperture*: The medium must be available in boules of diameter suitable for apertures characteristic of fusion-oriented CO_2 laser systems, i.e., of order 30 cm.

(c) *Cost*: The cost of optical materials must be minimum consistent with effective operation. Room-temperature operation is desirable, but not necessary.

IV. EXPERIMENTAL RESULTS FOR AN INTERBAND ISOLATOR

A. Choice of rotator material

Measured values from several sources for the interband Verdet coefficients of 16 materials are summarized in Fig. 1, at room temperature where available. A comparison of the materials listed for the 10.6-μm wavelength is given in Table II.

In the last column of the table, Eq. (13′) is used to estimate the maximum carrier density which would give free-carrier rotation equal to 1% of the interband rotation.

Of all the listed materials, CdTe has by far the best V/α value, but suffers from a low Verdet coefficient. InSb is rejected because of two-photon absorption. InAs cannot be grown with sufficient purity, since stoichiometry defects with density of order 10^{17} cm^{-3} are currently unavoidable during growth. The lead salts are unstable due to interchange defects,[42] and are typically doped heavily p type to achieve stability of V_i against temperature variations.[37] In addition, all the compounds listed other than Ge are not available in apertures larger than a few centimeters. For these reasons, Ge was chosen for this study. The material employed was single-crystal Ge, with maximum donor or acceptor density less than 10^{12} cm^{-3}.

B. Magnetic field characterization

The isolator magnetic field was produced by a simple uncompensated solenoid with a winding length of 8.76 cm and a 2.54-cm bore radius. The coil factor was

$$K(0,0)=B_z(0,0)/I_0=7.22\pm0.07\ \text{GA}^{-1}. \tag{19}$$

The peak field available at $R=Z=0$ was 83 kG 438 μs after firing the associated 750-μF 5.5-kV capacitor bank.

The total Faraday rotation in an inhomogeneous magnetic field $B(R,Z)$ is given by (see Fig. 2)

$$\Phi(R,Z_0)=2V\int_0^{Z_0}B_z(R,Z)\,dZ. \tag{20}$$

In Fig. 3, the calculated normalized rotation integrals averaged over the length $2Z_0$ of the rotator boule are given for our solenoid as a function of radius. The nonuniformity of rotation, defined as

$$\delta(R,Z_0)=\frac{\Phi(R,Z_0)-\Phi(0,Z_0)}{\Phi(0,Z_0)}, \tag{21}$$

is plotted in Fig. 4. Appendix C contains a complete discussion of these plots. The plot in Fig. 4 shows that a rotator boule of length equal to the coil length gives the worst radial variation of specific rotation, while a boule of length greater than about 12 cm gives more uniform rotation than an infinitely thin boule, or disk. This is because it is the integral $\int B_z$ rather than B_z which must be radially uniform. For materials of low absorptivity,

TABLE II. Comparison of 10.6-μm interband candidate materials at room temperature.[a]

Material	Probable residual absorption	V_I (deg cm^{-1} kG^{-1})	V/α (deg kG^{-1})	n_0	m_{Ee}/m	E_g (eV)	N_e max, est. (10^{13} cm^{-3})
InSb	5	11.8	2.4	3.96	0.012	0.18	4.0
PbTe	70	2.9	0.04	5.4	0.22	0.25	450
PbSe	40	1.4	0.04	4.6	0.27	0.26	270
PbS	30	1.0	0.03	4.1	0.15	0.37	50
InAs	1.5	0.66	0.44	3.5	0.029	0.35	1
Ge	0.01	0.08	8.0	4.0	0.12	0.65	3.6
CdTe	0.0003	0.03	100	2.7	0.14	1.50	0.9

[a] Sources of data for Table II were Fig. 1 and Refs. 11 and 39–41.

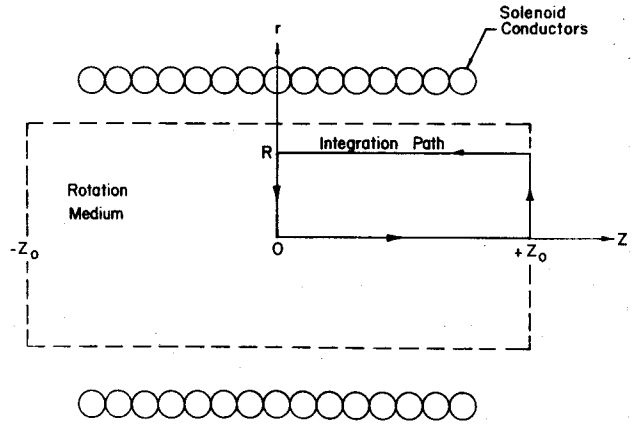

FIG. 2. Integration path for determining effect of magnetic field variations on uniformity of Faraday rotation.

this fact greatly relaxes the field homogeneity requirements, and permits more efficient use of the stored magnetic energy. For this reason, a germanium boule length $2Z_0 = 12$ cm was chosen for the isolator rotation medium in this study.

C. cw measurements setup

The experimental setup for cw measurements is indicated in Fig. 5. A chopped 0.5-W cw probe laser operating at 9.55- or 10.59-μm wavelength was the test signal source. The chopper provided a synchronization signal which permitted firing the pulsed solenoid at any time during a 1-ms test interval. The polarizer and analyzer were 4 plate germanium units with 51-dB crossed attenuation. These were roughly 1 m away from the solenoid on either side. The e^{-2} intensity diameter of the collimated probe beam in the rotator was 7.0 mm.

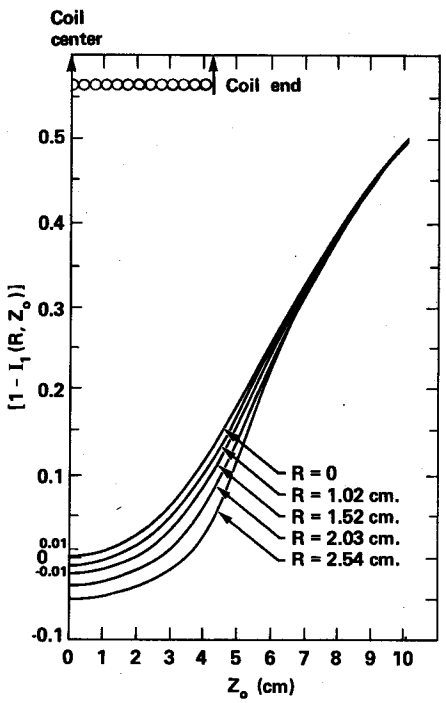

FIG. 3. Calculated radial and axial dependence of the specific rotation index I_1 in the LLL solenoid.

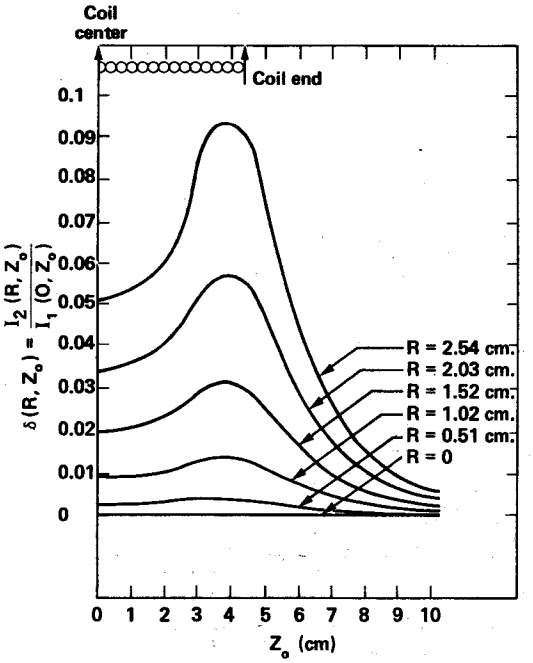

FIG. 4. Calculated radial and axial dependence of the rotation nonuniformity index I_2 in the LLL solenoid.

To prevent condensation on the polished and antireflection-coated end faces of the germanium boule, and to provide accurate temperature control, the chamber shown in Fig. 6 was used. The convex surface of the Ge cylinder was cooled by a Lauda chiller via a recirculating Freon "TF" bath, and the end faces were evacuated.

D. Interband verdet and isolation measurements

The procedure used in determining Verdet coefficients and the isolation level has been described previously.[25]

According to Eq. (13), the germanium interband Verdet coefficient should exhibit a λ^{-2} wavelength dependence in the $\omega \ll \omega_g$ limit. The wavelength dependence was checked at 9.55- and 10.59-μm wavelengths. At each of these wavelengths, the temperature dependence of the interband Verdet coefficient was measured for $260 \leq T \leq 300$ °K.

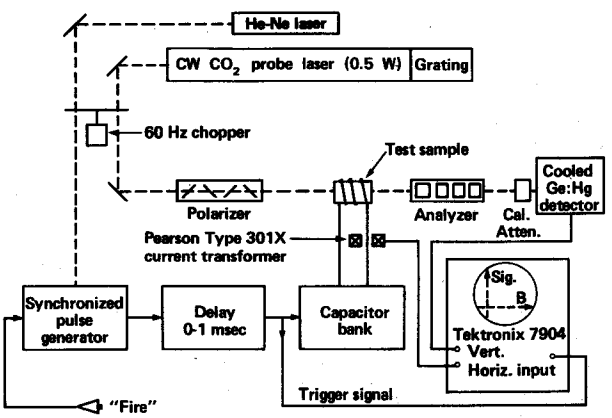

FIG. 5. Test setup for Verdet measurements.

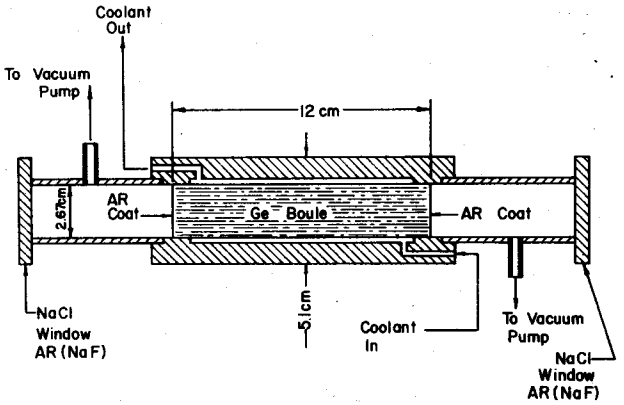

FIG. 6. Construction of test chamber for germanium rotation medium.

The results of measurements at the two wavelengths are shown in Fig. 7. The observed temperature and wavelength dependence is summarized in Table III. Included in the figure and table are the measured values of the isolation level or reverse attenuation, A. For these measurements, the Ge crystallographic orientation was such that $\mathbf{k} \| 100$.

Using Eq. (15) and Fig. 4, the rotation nonuniformity which can be ascribed to variations in the magnetic field within the 0.7-cm illuminated aperture corresponded to an isolation level of 53 dB. The radial nonuniformity index at $R = 0.8$ cm was measured by making an off-axis Verdet measurement. This result, shown in Table III, agrees well with Fig. 4. Had the entire Ge boule been illuminated, our calculations would predict a limiting isolation level due to field nonuniformity $A \cong 40$ dB. Therefore, field nonuniformity is not the primary factor limiting isolation to the 36-dB level observed.

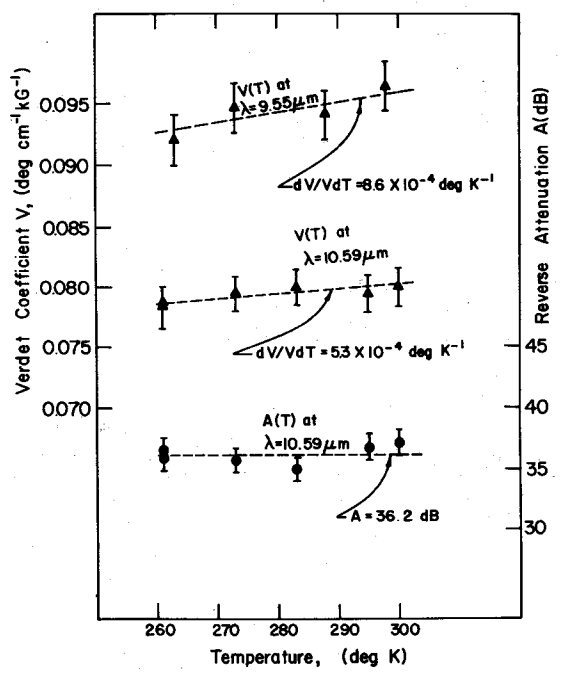

FIG. 7. Temperature dependence of the 9.55-μm and 10.59-μm Ge Verdet coefficient and of the 10.59-μm isolation level.

TABLE III. Verdet measurements at 9.55 and 10.59 μm. (Ge, $\mathbf{k} \| 100$, 0.5 W peak, 30 mW av, 7 mm illumination diameter).

	Wavelength 9.55 μm	10.59 μm	
$V(293\,°K)$	0.095 ± 0.002	0.080 ± 0.002	(deg kG^{-1} cm^{-1})
$\int_{-Z_0}^{+Z_0} B_Z dZ$ for $\Phi = 45°$	474 ± 9	563 ± 11	(kG cm)
W_m for $\Phi = 45°$	4.9 ± 0.2	7.0 ± 0.3	(kJ)
dV/VdT (260 $\leq T \leq$ 300)	$(8.6 \pm 3) \times 10^{-4}$	$(5.3 \pm 2) \times 10^{-4}$	(°K^{-1})
$\delta(0.8, Z_0)$	• • •	≤ 0.004	
$A(293\,°K)$	• • •	(36 ± 1)	(dB)

Measurements with polarizers crossed and $B = 0$ showed that any effects due to birefringence in the Ge crystal, or to depolarization by scattering from inhomogeneities, contribute an ellipticity no greater than − 50 dB.

The Verdet temperature dependence was somewhat smaller than would have been predicted from the energy gap temperature dependence alone. A $19 \pm 3\%$ variation in the Verdet coefficient between the two wavelengths is seen, whereas an ω^2 dependence would give a 23% change.

We note that the free-carrier rotation can account for no more than 1% of the measured rotation, and as little as 0.05% at the lowest temperature (see Sec. III E and Appendix B).

E. Linearity of rotation vs field

The approximations made in deriving Eqs. (6) and (13) give a linear dependence of θ on B in the limit of sufficiently small fields. Boswarva and Lidiard[15] predict perceptible saturation of θ/B in Ge on theoretical grounds, above fields of the order of 10 kG.

We checked to see whether nonlinear magnetorotation in Ge at 10.59 μm could be observed with field strengths as large as 83 kG. For this purpose, we measured the optical signal transmitted by a pure Ge test sample of length 5.72 cm, with crossed polarizers. Measurements were made as a function of coil current, and thus B, during each of several shots. The magnetic field nonuniformity was less than 1% within the test volume.

The setup shown in Fig. 5 was used. In this configuration, the cooled detector has no cw irradiation history prior to the test. Further, the cw probe laser was attenuated so that the maximum energy incident on the detector during each shot was 10^{-7} J. With these measures taken, the detector power law was linear. Using the measured room-temperature Verdet coefficient, $V(83\text{ kG}) = 0.08$, data were plotted vs $\sin^2(0.08 \int_{-Z_0}^{+Z_0} B\,dZ)$, as shown in Fig. 8. The slope of this log-log plot is 1.01 ± 0.01, demonstrating that the rotation is linear to within at least 1% up to 83-kG field intensities.

F. Absorption measurements

In order to calculate figure-of-merit values, mea-

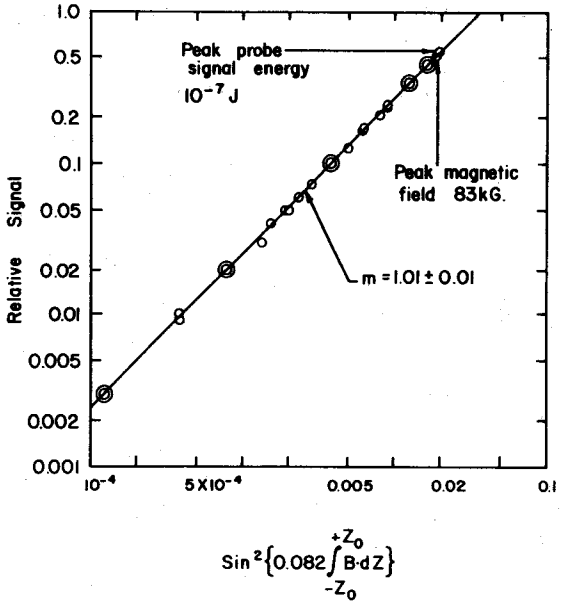

FIG. 8. Linearity of interband rotation in Ge for magnetic fields up to 83 kG.

surements were made to verify that free-carrier absorption in our Ge material agreed with the data of Bishop and Gibson.[48] The setup for absorption measurements is shown in Fig. 9. The calorimeters employed were twin IRTRAN-5 disk thermopiles designed and calibrated by Gunn[43,44] with a sensitivity of 0.70 and 0.31 μV mJ^{-1} and noise levels of 30 and 60 μJ, for the LC-7 and LC-7-1A instruments, respectively. Accuracy is 2% for the approximate energy range 1 mJ—1 J.[45] No more than 10 mJ per shot was absorbed by the Ge boule. The data points in Fig. 10 are the averaged result of approximately five shots at each temperature. The solid line shows the prediction of Bishop and Gibson, given by

$$\alpha(T)=\alpha_p+N_i(\sigma_h+\sigma_e), \tag{22}$$

where for $\lambda=10.59$ μm, $\alpha_p=0.013$ cm^{-1}, $\sigma_h=6.5\times10^{-16}$ cm^2, $\sigma_e=0.15\times10^{-16}$ cm^2, and N_i is the intrinsic concentration given by Eq. (B1). It is seen that sufficient agreement is obtained to permit using the Bishop and Gibson data to predict $\alpha(T)$.

For 45° rotation and a 12-cm sample length, the low-intensity low-field figure of merit in Ge is given for $\lambda=10.59$ μm by

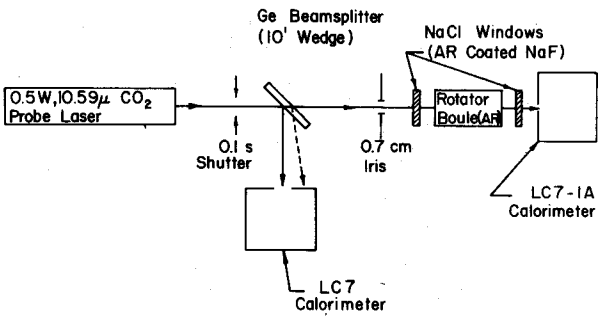

FIG. 9. Test setup for absorption measurements.

$$Q(T)=[0.863/\alpha(T)]\ \text{deg dB}^{-1}. \tag{23}$$

At high intensities, the hole transition absorption bleaches (refer to Appendix A 1), leaving the residual absorption $\alpha_0(T)$ and nearly constant merit figure $Q_0(T)$, plotted in Fig. 10.

G. Tests with nanosecond-duration pulses

To check the isolation level at high intensities, the cw laser and chopper shown in Fig. 5 were replaced by an actively mode-locked oscillator and single-pulse switchout of the type described in Ref. 46. In this configuration, the probe signal at the isolator was a single pulse with duration about 2 ns at the 10.59-μm wavelength, a beam waist diameter of 7 mm, and an intensity of about 1 MW cm^{-2}. On successive shots, the transmitted intensity was measured vs laser pulse delay at room temperature. Figure 11 shows the result of these measurements. The maximum isolation level recorded was about 41 dB.

V. DISCUSSION

We have described the construction and testing of a high-power isolator for the 10-μm region, based on interband Faraday rotation in intrinsic Ge. The isolation level of this device is in excess of 40 dB at a single wavelength and is quite uniform radially, in a field provided by a simple uncompensated solenoid. The quadratic dependence of rotation on wavelength would limit the device isolation to about 30 dB for simultaneous

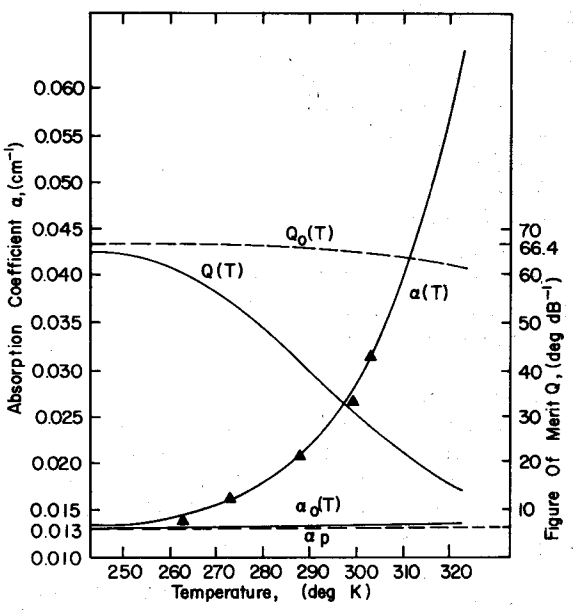

FIG. 10. Comparison of experimental data points (Δ) with calculation based on data of Bishop and Gibson (Ref. 48) and temperature dependence of low-intensity low-field absorption in Ge. α_p is the phonon absorption coefficient, and α_0 is the residual absorption after bleaching of the hole transition absorption. Also shown are the figures of merit predicted for a 12-cm interband rotator using the total and residual absorption coefficients.

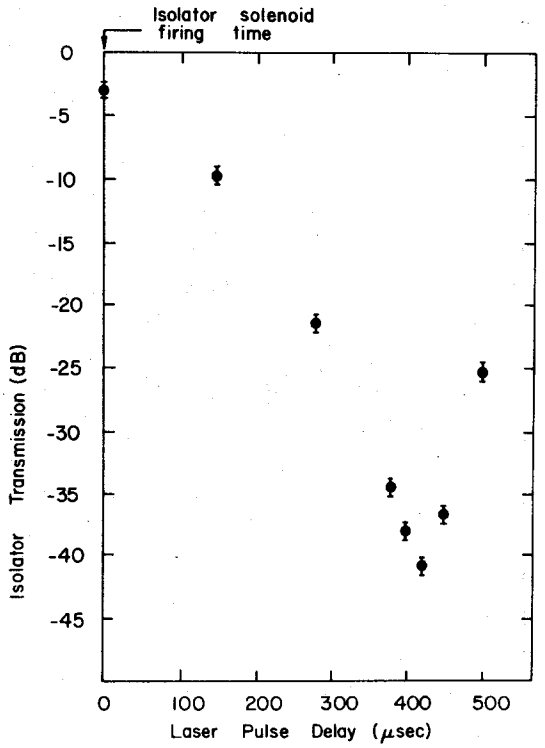

FIG. 11. Isolation level vs delay time for nanosecond duration 10.59-μm pulses.

signals at the 9.5- and 10.6-μm CO_2 wavelengths. The observed isolation level is probably determined by magnetically induced differential absorption of the rcp and lcp components (refer to Appendix A1). By referring to Eq. (A1), it is seen that a difference $\alpha_+ - \alpha_- = 0.003$ cm^{-1} is sufficient to give the 41-dB isolation level observed in the nanosecond pulse tests. We could not accurately measure such a small difference. However, significant enhancement of the hole transition absorption for plane-polarized waves was observed for the highest magnetic fields used, and will be reported at a later date. This magnetically induced absorption is also bleachable, and has no effect on $Q_0(T)$ in Fig. 10. Nonuniform heating plays an insignificant role since no temperature dependence of the isolation level was seen within experimental accuracy.

The measurements reported in Ref. 25, using the 112 crystallographic orientation in Ge, and the present measurements show no difference in the Verdet coefficient within the experimental error of 2%. This result suggests that polycrystalline material would at least give an isolation level of 36 dB.

The measured Verdet coefficient shows the correct frequency dependence, a very weak temperature dependence, and is in excellent agreement with previous measurements at shorter wavelengths.

The primary practical advantages of our isolation device are as follows: (i) availability of the rotation medium in large apertures; (ii) applicability to high-power laser systems in the 10-μm region; (iii) room-temperature operation; (iv) superior isolation levels achievable in a single unit; and (v) good figure of merit, for economy of laser energy.

VI. DIRECTIONS FOR FUTURE WORK

For high-power applications, this isolator is apt to be limited by the surface burn threshold of antireflection-coated germanium. Coatings must be developed to extend this limit at least a factor of 5 beyond the present level, estimated to be 5×10^8 W cm^{-2}. Planned tests at gigawatt/cm^2 intensities will also show whether nonlinear optical processes cause beam quality deterioration.

Another important problem is the design of economical large-aperture polarizers. The Brewster-angle Ge plate polarizers used for these measurements become costly at large apertures, since the plate surfaces must be flat to within about 0.1 μm for diffraction-limited propagation.

The major cost item in a germanium interband isolator is the magnetic field source. Operation at 9.5-μm wavelength would reduce this cost by about 50%.

ACKNOWLEDGMENTS

The authors are grateful to Professor B. Lax of MIT for suggesting the use of interband rotation for high-power isolators. They also wish to thank Dr. K. R. Manes and Dr. H. Ahlstrom of the Lawrence Livermore Laboratory and Dr. S. Singer and Dr. J. F. Figueira of the Los Alamos Scientific Laboratory for numerous discussions, interest, and support for this research. Dr. G. Armantrout of the Lawrence Livermore Laboratory provided germanium of extremely high purity for the rotation medium, which greatly facilitated the authors' work.

APPENDIX A: DISCUSSION OF EFFECTS WHICH LIMIT THE INTERBAND ISOLATION LEVEL

Assuming a uniform magnetic field, interband device isolation levels will be limited by three effects.

1. Ellipticity induced by differential absorption

This effect is related to the difference in the absorption coefficients $\alpha_\pm$ for rcp and lcp waves. The ellipticity is

$$\rho_\alpha = \left(\frac{I_\perp}{I_0}\right)^{1/2} = \tanh\left[\left(\frac{\alpha_+ - \alpha_-}{2}\right) Z_0\right] \qquad \text{(A1)}$$

where $2Z_0$ is the sample length. In an intrinsic semiconductor well below the gap frequency, the residual absorptions are due to (i) phonon or lattice absorption and (ii) intraband absorption. Since (i) should not exhibit circular dispersion, intraband effects dominate Eq. (A1).

Intraband absorption in Ge is composed of two parts for wavelengths in the range 5—100 μm, that due to transitions between the degenerate heavy and light hole bands, and that due to free-electron absorption.[47] In intrinsic material at 10.6 μm, the ratio of these absorptions is the ratio of their cross sections, $\sigma_h/\sigma_e = 43$.[48] Since the hole transition absorption will bleach at intensities in excess of 10 MW cm^{-2},[49] only 2.3% of the low-power ellipticity should remain at high power

levels. The residual phonon absorption at 10.6 μm is 0.013^{-1},[48] but should exhibit no circular dispersion.

2. Ellipticity due to the Voigt effect

The phase shift $\delta = k(n_{\parallel} - n_{\perp})$ due to the Voigt effect is a birefringence which is quadratic in $|\hat{\mathbf{k}} \times \mathbf{B}| = B_r$. The ellipticity ratio due to this effect is given by

$$\rho_v = (I_\perp / I_0)^{1/2} = \tan(\delta Z_0). \tag{A2}$$

In the low-frequency limit, the interband Voigt shift for $B_r = B_z$ is related to the specific rotation by[10]

$$\frac{\delta}{\theta} \approx \frac{1}{80}\left(\frac{g_c + g_v}{2}\right) \frac{\omega \omega_c}{\omega_g^2} \tag{A3}$$

For example, with Ge at $B = 80$ kG, $\omega\omega_c\omega_g^{-2} \approx 0.01$, giving $\delta/\theta \approx 10^{-3}$, which corresponds to an isolation limit of $A \approx 47$ dB, when $2Z_0 = 12$ cm. In our experiment, $B_r \ll B_z$, so that Voigt ellipticity is negligible.

3. Spacial effects of nonuniform heating

Since we are assuming a pure semiconductor medium in which free-carrier rotation can be ignored, heating will affect the rotation uniformity mainly through local energy gap variations. These can be estimated by referring to Eq. (13). In germanium, $d\omega_g/\omega_g dT = -3.9 \times 10^{-4}\,^\circ\mathrm{K}^{-1}$.[50] If other parameters in Eq. (13) are assumed constant, we should have $dV/V\,dT \leq 8.6 \times 10^{-4}\,^\circ\mathrm{K}^{-1}$. There fore, from Eq. (15), a 10 °K temperature variation across the aperture of a germanium rotator crystal would limit the achievable isolation level to 43 dB.

APPENDIX B: DISCUSSION OF GERMANIUM PURITY REQUIREMENTS

In germanium, the temperature dependence of the intrinsic free-carrier density is given by[13]

$$N_i(T) = 1.76 \times 10^{16} T^{1.5} \exp(-4555/T)\ \mathrm{cm}^{-3}. \tag{B1}$$

Inserting this result and $m_{Fe}/m = 0.12$ and $m_{Fp}/m = 0.25$ for the conductivity effective masses of electrons and holes in Ge[13] into Eq. (13′), we find

$$V_F(\mathrm{Ge}) = 0.00355 \lambda_\mu^2 T^{1.5} \exp(-4555/T)\ \mathrm{deg\,cm^{-1}\,kG^{-1}} \tag{B2}$$

for the free-carrier Verdet coefficient in intrinsic Ge. Since $V_I = 0.08$ deg cm^{-1} kG^{-1} at 10.6 μm,[25] the requirement that $V_I/V_F \geq 100$ implies $T \leq 308$ °K for pure material, or that $N \leq 3.6 \times 10^{13}$ cm^{-3} for an impurity specification.

Note that, using the Bishop and Gibson absorption data,[48] the zero-field free-carrier component of α for intrinsic Ge is

$$\alpha_F = N_i(\sigma_h + \sigma_e) = 11.7 T^{1.5} \exp(-4555/T)\ \mathrm{cm}^{-1}. \tag{B3}$$

This becomes equal to the phonon absorption $\alpha_p = 0.013$ cm^{-1} at $T = 297$ °K, or for $N_i \cong 2.0 \times 10^{13}$ cm^{-3}.

APPENDIX C: CHARACTERIZATION OF ROTATION UNIFORMITY

For field source driving frequencies ω small enough that both displacement currents $(1/4\pi)(\partial \mathbf{D}/\partial t)$ and induced Ohmic currents J in the rotator medium can be ignored relative to Ohmic currents in the field source, Maxwell's equations guarantee that the line integral of the field along any closed path within the field source, in a medium of uniform relative permeability μ, is zero:

$$\oint \mathbf{B} \cdot d\mathbf{s} = 0. \tag{C1}$$

For the foregoing assumptions to be valid, we note that displacement current will be smaller than induced Ohmic currents in the medium if

$$\rho < 1.1 \times 10^9 \omega^{-1} \epsilon^{-1}\ \Omega\,\mathrm{cm}, \tag{C2}$$

where ϵ is the dielectric constant. Ohmic currents in the medium will in turn be smaller than the excitation current for times much longer than a characteristic field penetration time τ_p, given for a long cylinder of radius R by[51]

$$\tau_p = 3.2[R^2\ (\mathrm{cm})/\rho\ (\Omega\,\mathrm{cm})]\ \mathrm{ns}. \tag{C3}$$

Our experimental parameters were $\omega = 3285$ s^{-1}, time to peak field $t_0 = 438$ μs, rotator resistivity $\rho \cong 40\ \Omega$ cm, $\epsilon = 16$, and radius $R = 1.34$ cm.

With these parameters, Eq. (C2) requires that $\rho < 2 \times 10^4\ \Omega$ cm, and Eq. (C3) that $t_0 > 0.14$ ns. Therefore, the assumptions made in writing Eq. (C1) are accurate to order 10^{-6}.

Along the midplane of an axisymmetric field source (e.g., a simple solenoid), $B_r(r, 0) = 0$. Therefore, where Eq. (C1) holds, the radial nonuniformity of rotation is given by

$$\Phi(R, Z_0) - \Phi(0, Z_0) = 2V\left[\int_0^{Z_0} B_z(0, Z)\,dZ - \int_0^{Z_0} B_z(R, Z)\,dZ\right] = 2V \int_0^R B_r(r, Z_0)\,dr. \tag{C4}$$

Accordingly, we define two integrals I_1 and I_2 which will facilitate calculation of both the spatial average specific rotation and the nonuniformity of rotation in an inhomogeneous but axially symmetric stationary field:

$$I_1(R, Z_0) = [Z_0 B_z(0, 0)]^{-1} \int_0^{Z_0} B_z(R, Z)\,dZ, \tag{C5}$$

$$I_2(R, Z_0) = [Z_0 B_z(0, 0)]^{-1} \int_0^R B_r(r, Z_0)\,dr. \tag{C6}$$

In terms of these integrals, which are readily calculated from measured field profiles, we obtain the total rotation and the rotation nonuniformity index:

$$\Phi(R, Z_0) = 2 Z_0 V B_z(0, 0) I_1(R, Z_0), \tag{C7}$$

$$\delta(R, Z_0) = \frac{\Phi(R, Z_0) - \Phi(0, Z_0)}{\Phi(0, Z_0)} = \frac{I_2(R, Z_0)}{I_1(0, Z_0)}. \tag{C8}$$

Note that

$$\lim_{Z_0 \to \infty} I_2(R, Z_0) = \lim_{Z_0 \to \infty} I_1(R, Z_0) = 0 \tag{C9}$$

for any path such that $R < R_0$. The quantity $[I - I_1]$ plotted in Fig. 3 gives the fractional increase in solenoid excitation which would achieve the same total rotation at radius R in a boule of length $2Z_0$ as would be achieved with a uniform field $B = B_z(0, 0)$. Since $\delta(R, Z_0)$ is plotted directly in Fig. 4, achievable isolation levels may be calculated from the plot, as a function of radius and boule length.

*Work supported by the U. S. Energy Research and Development Administration.
†The work described in this paper was performed in part while both authors were at the Lawrence Livermore Laboratory, Livermore, CA.

[1]J. L. Emmett, J. Nuckolls, and L. Wood, Sci. Am. 230, 24 (1974).
[2]O. C. Barr, J. M. McMahon, and J. B. Trenholme, IEEE J. Quantum Electron. QE-9, 1124 (1973).
[3]Lawrence Livermore Laboratory Report No. UCRL-50021-73-2, p. 50, 1974 (unpublished).
[4]G. T. Schappert and E. E. Stark, Jr., Appl. Phys. Lett. 25, 602 (1974).
[5]R. E. Jensen and M. S. Tobin, IEEE J. Quantum Electron. QE-8, 34 (1972).
[6]D. L. Smith and D. T. Davis, IEEE J. Quantum Electron. QE-10, 138 (1974).
[7]J. H. Dennis, IEEE J. Quantum Electron. QE-3, 416 (1967).
[8]W. T. Boord, Y. H. Pao, F. W. Phelps, Jr., and P. C. Claspy, IEEE J. Quantum Electron. QE-10, 273 (1974).
[9]W. E. Bicknell, L. R. Tomasetta, and D. H. Bates, VIII International Quantum Electronics Conference, San Francisco, 1974, Paper X-11 (unpublished).
[10]B. Lax and J. G. Mavroides, in *Semiconductors and Semimetals*, *Vol.* 3 (Academic, New York, 1967).
[11]T. S. Moss, *Optical Properties of Semiconductors* (Butterworths, London, 1961).
[12]H. Becquerel, C. R. Acad. Sci. Paris 125, 679 (1897).
[13]Since mobility μ is defined in terms of a collision time τ, the factor $g = \langle\tau\rangle\langle 1/\tau\rangle$ is necessary. See R. A. Smith, *Semiconductors* (Cambridge U. P., London, England, 1964).
[14]L. M. Roth, Phys. Rev. 133, A 542 (1964).
[15]I. M. Boswarva and A. B. Lidiard, Proc. R. Soc. A 278, 588 (1964).
[16]J. Halpern, B. Lax, and Y. Nishina, Phys. Rev. 134, A140 (1964).
[17]J. Kolodziejczak, B. Lax, and Y. Nishina, Phys. Rev. 128, 2655 (1962).
[18]Excellent reviews of Faraday rotation theory and experiments are contained in Ref. 10 and in S. D. Smith, in *Encyclopedia of Physics*, Vol. XXV/2a (Springer Verlag, Berlin, 1967); Y. I. Ukhanov, Sov. Phys.-Usp. 16, 236 (1973); and M. Balkanski and E. Amzallag, Phys. Status Solidi 30, 407 (1968).
[19]H. Piller, in *Semiconductors and Semimetals*, *Vol.* 8 (Academic, New York, 1972).
[20]A. K. Walton and U. K. Mishra, Proc. Phys. Soc. (Lond.) 90, 1111 (1967).
[21]B. Lax, *Proceedings of the International School of Physics "Enrico Fermi," Course* 22 (Academic, New York, 1963), p. 240.
[22]I. M. Boswarva, R. E. Howard, and A. B. Lidiard, Proc. R. Soc. A 269, 125 (1962).
[23]H. S. Bennett and E. A. Stern, Bull. Am. Phys. Soc. 5, 279 (1960).
[24]T. F. Deutsch, U. S. Army Missile Command Contract No. DA AH01-72-C-0194 Final Report, 1973 (unpublished).
[25]C. R. Phipps and S. J. Thomas, Appl. Phys. Lett. 25, 313 (1974).
[26]S. D. Smith, C. R. Pidgeon, and V. Prosser, in *Proceedings of the International Conference on the Physics of Semiconductors Exeter* (Institute of Physics, London, 1962), p. 301.
[27]S. D. Smith, T. S. Moss, and K. W. Taylor, J. Phys. Chem. Solids 11, 131 (1959).
[28]J. M. Doviak, A. F. Gibson, M. F. Kimmitt, and A. C. Walker, J. Phys. C 6, 593 (1973).
[29]S. D. Jacobs, K. J. Teegarden, and R. K. Ahrenkiel, Appl. Opt. 13, 2313 (1974).
[30]A. Ebina, T. Koda, and S. Shionoya, J. Phys. Chem. Solids 26, 1497 (1965).
[31]M. Zvara, F. Zaloudek, and V. Prosser, Phys. Status Solidi 16, K21 (1966).
[32]H. Piller, *Proceedings of the International Conference on Semiconductors Paris* (Academic, New York, 1964), p. 297.
[33]T. S. Moss and B. Ellis, Proc. Phys. Soc. (Lond.) 83, 217 (1964).
[34]H. Piller and V. A. Patton, Phys. Rev. 129, 1169 (1963).
[35]A. K. Walton and T. S. Moss, Proc. Phys. Soc. (Lond.) 78, 1393 (1961).
[36]C. J. Summers and S. D. Smith, Proc. Phys. Soc. (Lond.) 92, 215 (1967).
[37]M. S. Kozyreva, Sov. Phys.-Semicond. 4, 986 (1970).
[38]C. J. Gabriel, Phys. Rev. B 2, 1812 (1970).
[39]N. K. Abrikosov, V. F. Bankina, L. V. Poretskaya, L. E. Shelimova, and E. V. Skudnova, *Semiconducting II-VI, IV-VI and V-VI Compounds* (Plenum, Oxford, England, 1969).
[40]J. T. Houghton and S. D. Smith, *Infrared Physics* (Clarendon, Oxford, 1966).
[41]J. Kolodziejczak, Acta Phys. Polon. 20, 289 (1961).
[42]W. L. Hansen (private communication).
[43]S. R. Gunn, J. Phys. E 6, 105 (1973).
[44]Lawrence Livermore Laboratory Report No. UCRL-50021-72-1, p. 95, 1972 (unpublished).
[45]This figure is based upon the quoted noise level. The calibration factor was determined by resistance heating at 20 °C. An allowance of 0.7% for reflected energy is incorporated in the factor. The standard deviation of energy readings from electrical resistance inputs is typically 1%.
[46]Lawrence Livermore Laboratory Report No. UCRL-50021-72-2, p. 20, 1972 (unpublished).
[47]A. H. Kahn, Phys. Rev. 97, 1647 (1955).
[48]P. J. Bishop and A. F. Gibson, Appl. Opt. 12, 2549 (1973).
[49]A. F. Gibson, C. A. Rosito, C. A. Raffo, and M. F. Kimmitt, Appl. Phys. Lett. 21, 356 (1972).
[50]S. Zwerdling, B. Lax, L. M. Roth, and K. J. Button, Phys. Rev. 114, 80 (1959).
[51]R. V. Churchill, *Fourier Series and Boundary Value Problems* (McGraw-Hill, New York, 1941).